Cascaded ”Triple-Bent-Beam” MEMS Sensor for Contactless Temperature Measurements in Nonaccessible Environments

Carlo Trigona, Salvatore Baglio, Bruno Andò, Nicolò Savalli

To cite this version:

Carlo Trigona, Salvatore Baglio, Bruno Andò, Nicolò Savalli. Cascaded ”Triple-Bent-Beam” MEMS Sensor for Contactless Temperature Measurements in Nonaccessible Environments. IEEE Transactions on Instrumentation and Measurement, 2011, 60 (4), pp.1348-1357. 10.1109/TIM.2010.2101310. lirmm-00580551

HAL Id: lirmm-00580551
https://hal-lirmm.ccsd.cnrs.fr/lirmm-00580551

Submitted on 28 Mar 2011

Cascaded “Triple-Bent-Beam” MEMS Sensor for Contactless Temperature Measurements in Nonaccessible Environments

Bruno Andò, Salvatore Baglio, *Senior Member, IEEE*, Nicolò Savalli, and Carlo Trigona

***Abstract*—A microelectromechanical systems (MEMS) temperature sensor based on a cascade three-stage “bent-beam” structure is described in this paper. A suspended structure mechanically deforms in response to the change in ambient temperature, and then, a displacement is obtained; the structure is composed of three cascaded systems in order to enhance sensor sensitivity. The final conversion is made to an electrical signal that is obtained by using an interdigitated capacitor having one electrode fixed to the substrate and one electrode embedded into the moving tip of the MEMS sensor. The device has been conceived to operate passively in harsh environments where high temperatures could harm active electronic devices. The readout of the unknown temperature is therefore remotely performed by coupling the variable MEMS capacitor to a fixed inductor to compose a resonant LC circuit, which is magnetically coupled to a reader circuit placed outside the environment where the measurement takes place. The temperature to be measured is therefore first converted into a displacement that, in turn, induces a change in a capacitor value; a variation in the resonant frequency of an LC circuit is finally observed through the remote readout circuit. This paper focuses on the analytical and numerical modeling of both the temperature-to-displacement and displacement-to-capacitance conversions, on the design and fabrication of an experimental prototype, on the experimental validation where results are extensively presented and commented, and, finally, on the design of the integrated resonant device for contactless measurements.**

***Index Terms*—Bent-beam structures, contactless sensors, microelectromechanical systems (MEMS), temperature sensors.**

I. INTRODUCTION

SEVERAL SCENARIOS exist where a cabled connection between the primary sensor and the signal conditioning circuit is not allowed. Contactless measurement strategies can therefore be adopted to gather information from sensors used in hostile or inaccessible areas. The literature offers many examples and many application fields for remote and contactless sensors; examples are remote data acquisition from an autonomous sensor module based on an optical link [1], pressure sensors in microelectromechanical systems (MEMS) technology for high-temperature applications [2], contactless sensors for biomedical applications [3], and chemical sensors for high-temperature environments [4].

A particular situation could arise when the measurement environment is unsuitable for electronic circuitry due to high temperatures and the temperature itself is the quantity to be measured. Solutions to this problem are required not only in the area of process control but also in risk prevention and contingency management and whenever a sensor is required to be placed inside the environment. High-temperature rooms, industrial ovens, or, generally speaking, environments that are incompatible with either wire or active electronic parts are some examples.

A typical approach to the problem of remote temperature sensing relies on radiation-based thermometers; however, small low-cost devices that can easily be placed inside the measurement environment are of great interest.

A temperature sensor for applications in such environments must show a large operating range and the capability to transfer the information without wired connections, onboard power supply, and active electronic components.

From this perspective, MEMS technology allows suitable solutions providing different materials that are compatible with high-temperature environments and that allow for the implementation of contactless reading mechanisms.

Several designs and procedures for the fabrication and testing of microfabricated mechanical temperature sensors have been presented in the literature [5], with a variety of architectures [6]. The common working principle is based on the structural deformation that appears as a consequence of a temperature increase.

In this paper, a novel contactless temperature sensor is developed. It is based on an array of V-shaped bent-beam structures [7]. Similar structures have been previously proposed in the literature mainly as in-plane thermal actuators [7]–[11] or strain sensors [12], [13]; here, the remote sensing of environment temperature is addressed.

A cascade triple-beam architecture has been designed in order to enhance the sensitivity of the sensor. A passive remote readout system, based on an LC resonant architecture with varying capacitor, which produces a frequency shift as output in response to the temperature change, has been conceived. Therefore, wires, contacts, active elements, and power supplies within the sensor have been removed. Some preliminary results on the sensor characterization have been previously reported

Manuscript received November 4, 2009; revised March 12, 2010; accepted March 25, 2010. The Associate Editor coordinating the review process for this paper was Dr. Thomas Lipe.

The authors are with the Dipartimento di Ingegneria Elettrica Elettronica e dei Sistemi, University of Catania, 95125 Catania, Italy (e-mail: salvatore.baglio@diees.unict.it).

Color versions of one or more of the figures in this paper are available online at http://ieeexplore.ieee.org.

Digital Object Identifier 10.1109/TIM.2010.2101310

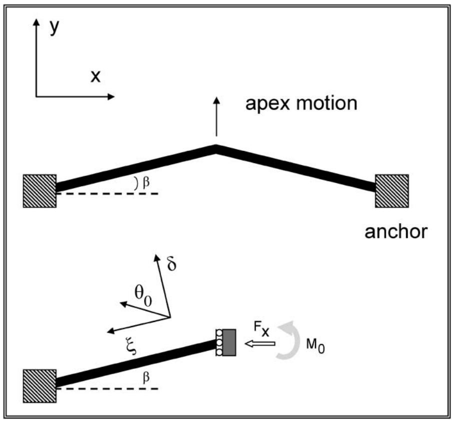

Fig. 1. Structure and operation of a single-bent-beam sensor.

by the authors in [14], while some results on a hybrid solution for the wireless sensor readout have been also presented in [15] where the MEMS sensor is used in a system including an external printed circuit board coil.

Here, both a more exhaustive characterization and a more accurate modeling of the MEMS device are presented.

The MEMS sensor has been designed so that the temperature induces a displacement of one conductive electrode (the tip of the cascaded triple bent beam) toward a fixed electrode, thus realizing a variable capacitor that is coupled with an embedded coil inductor [14]. This LC circuit will respond, when remotely interrogated, with a resonance frequency that is a function of the capacitance value which, in turn, depends on the temperature to be measured [15].

An accurate analytical model of the proposed device, together with the actual design realized with the MetalMUMPs technology [16], is presented in this paper. In particular, an accurate analysis of the nonideal characteristics of the MEMS sensor will be developed here, leading to a better comprehension of some unexpected behaviors. Finally, extensive simulation and experimental results, obtained by using the designed and fabricated prototype, will be reported to validate the approach discussed here.

II. DEVICE MODELING

A reference bent-beam device is shown in Fig. 1. It is composed of a V-shaped beam anchored at the two ends. The thermal expansion of the structure induces a displacement of the central apex along the y-direction. Owing to its symmetry, this is the only possible direction of deformation for the device considered.

Because of the system symmetry, it is sufficient to analyze only one-half of the structure. In order to determine the free displacement, the beam can be considered as subjected to an equivalent force that causes the free expansion at the apex. Flexure symmetry is also useful to determine the boundary conditions. Displacements and rotations of the beam ends are constrained to be zero, except in the direction of the applied force, and the boundary conditions are determined by solving the equilibrium equations $\Sigma F = 0$, $\Sigma M = 0$, and $\Sigma T = 0$, where F, M, and T are the forces, the moments, and the torques applied to the structure, respectively.

These boundary conditions are expressed in terms of the reaction forces, moments, and torsions at the end of the beam. Finally, Castigliano's second theorem [17] states that the partial derivative of the strain energy U of a linear structure, with respect to a given load P, is equal to the displacement δ of the point where the load is applied. This theorem can be extended to the applied moments M and their corresponding angular displacements θ, resulting in

$$\delta = \frac{\partial U}{\partial P} \quad \theta = \frac{\partial U}{\partial M}. \tag{1}$$

In applying Castigliano's theorem, the strain energy must then be expressed as a function of the load. If, for example, a straight bar subjected to a number of common loads (axial force N, bending moment M, shearing force V, and torque T) is considered, the strain energy has the following form:

$$U = \int \frac{N^2}{2AE}\,dx + \int \frac{M^2}{2EI}\,dx + \int \frac{\alpha V^2}{2AG}\,dx + \int \frac{T^2}{2JG}\,dx \tag{2}$$

where A is the cross-sectional area, G and J are the torsion modulus and the torsion constant, respectively, the product EI is called the flexural rigidity of the beam, E is the Young's modulus of elasticity, α is a coefficient depending on the cross-sectional shape [18], and I is the bending moment of inertia.

By focusing on the subject of this paper, only the displacements resulting from bending are considered in the analysis, whereas deformations from shear, beam elongation, and shortening are neglected; the strain energy of the beam is found by integrating the strain energy density along the beam

$$U = \int_0^L \frac{M^2}{2EI} d\xi. \tag{3}$$

The ξ-coordinate points along the beam axis, while L is the length of the beam. The angle at the fixed end of the beam θ_0 is fixed at zero by the symmetry of the flexure. An external bending moment M_0 constrains the angle in the analysis. The beam bending moment is

$$M = M_0 - F_y \xi \tag{4}$$

where ξ is along the beam (x-axis) and F_y is along y.

A first invocation of Castigliano's second theorem gives a relation between the external moment and the load

$$\theta_0 = \frac{\partial U}{\partial M_0} = \frac{1}{EI}\int_0^L M \frac{\partial M}{\partial M_0} d\xi = \frac{1}{EI}\int_0^L (M_0 - F_y \xi) d\xi. \tag{5}$$

That, combined with the constraint $\theta_0 = 0$, gives $M_0 = F_y L/2$.

The displacement along the y-direction δ_y can be obtained as

$$\delta_y = \frac{\partial U}{\partial P} = \frac{1}{EI}\int_0^L M \frac{\partial M}{\partial P} d\xi = \frac{1}{EI}\int_0^L F_y \left(\frac{L}{2} - \xi\right) d\xi \tag{6}$$

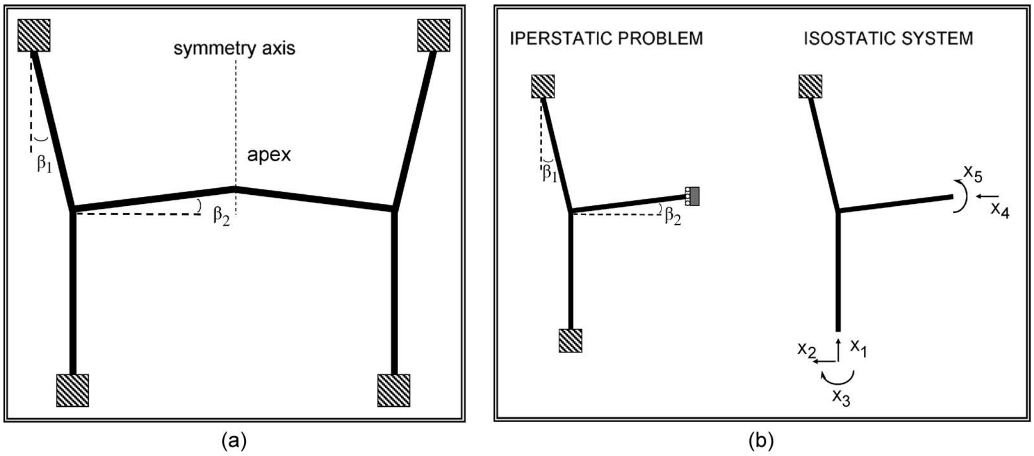

Fig. 2. (a) Structure of a cascaded (triple) bent-beam sensor. (b) Iperstatic problem and equivalent isostatic system.

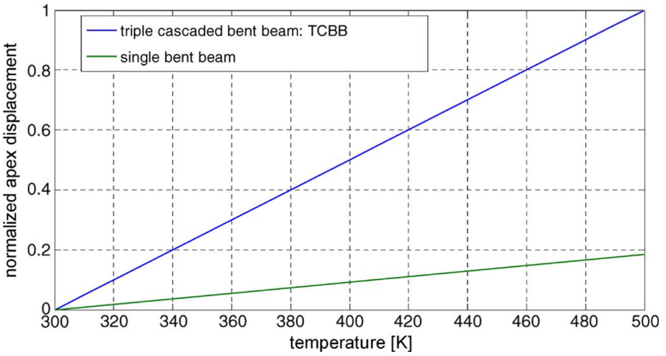

Fig. 3. “Normalized apex displacement” versus temperature. Comparison between the single bent beam and the cascaded bent beam (triple).

then

$$\delta_y = F_y \frac{L^3}{12EI}. \tag{7}$$

The last step is to derive the moment of inertia $I = I_{zz} = I_{xx} + I_{yy}$, where

$$I_{xx} = \int_{-L/2}^{+L/2} \frac{A}{L} x^2 \sin^2(\beta) dx = \frac{AL^2}{12} \sin^2(\beta) \tag{8}$$

$$I_{yy} = \int_{0}^{L} \frac{A}{L} \xi^2 dy = \frac{AL^3}{3} \cos^2(\beta) = I_z \cos^2(\beta). \tag{9}$$

Finally

$$\delta_y = F_y \frac{L^3}{12E(I_{xx}+I_{yy})} = \frac{F_y L^3}{12EI_z \cos^2(\beta) + AEL^2 \sin^2(\beta)} \tag{10}$$

where $F_y = \alpha\ EA\ \Delta T \sin\beta$ is the y-component of the axial equivalent force related to the temperature change ΔT.

The equation indicates that the displacement at the apex depends linearly on the temperature increase and nonlinearly on the geometric parameters defining the half bent beam.

The resultant in-plane displacement of a central apex can be increased by cascading several elementary V-shaped bent beams as shown in Fig. 2(a) for the case of a cascaded (triple) bent-beam sensor.

A more general approach has been considered in this case to analytically model the device. The virtual work principle [17] has been applied to derive the displacement of the apex for the triple cascaded bent beam (TCBB), shown in Fig. 2(a). As with the simpler structure described previously, symmetry allows the analysis of only half the structure.

By starting from an iperstatic structure, it is possible to study the isostatic system in which five reaction forces act on the suppressed constraints, to satisfy both equilibrium and congruency conditions, as shown in Fig. 2(b).

As for the case of the single bent beam, the model evinces a linear dependence of the apex displacement δ_y on the temperature ΔT; in particular, the displacement of the apex can be expressed as follows [17]:

$$\begin{aligned}\delta_y = &- \frac{1}{2EI} L^3 X_1 \left[\cos(\beta_1)\sin(\beta_1) + \cos^2(\beta_2)\right] \\ &+ L^3 X_2 \cos^2(\beta_1) - L^2 X_3 \cos(\beta_1) + \frac{L^3}{2} X_4 \cos^2(\beta_2) \\ &+ L^2 X_5 \left(\cos^2(\beta_1) + \frac{\cos(\beta_2)}{2}\right)\end{aligned} \tag{11}$$

where X_1, X_2, X_3, X_4, and X_5 are the aforementioned reaction constraint forces that are determined separately.

The equations obtained allow the evaluation of the differences between the single and the cascade structures in terms of sensitivity to the external temperature: Sensitivity is strongly enhanced with the proposed TCBB configuration, as shown in Fig. 3 (the results are normalized due to their dependence on the geometrical features of the structures).

The idea developed in this work is that the deformation of the structure, due to a change in the environment temperature, and the resulting displacement of the apex is measured as a variation in capacitance if a suitable electrical component is placed on top of the moving tip of the structure; an interdigitated comb capacitor has been used for this purpose. The change in the capacitance can therefore be used as a resonant LC circuit to implement a contactless readout strategy.

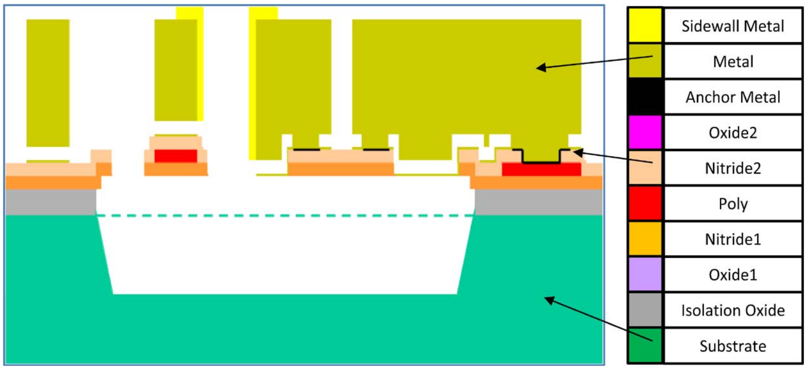

Fig. 4. MetalMUMPs process cross section.

III. MICROFABRICATION TECHNOLOGY, WORKING PRINCIPLE, AND SIMULATION RESULTS

Electroplated nickel cascaded bent beams have been realized by using the high-aspect-ratio MetalMUMPs process [16] provided by MEMSCAP.

The device is built directly over a silicon nitride isolation layer with a 1-μm air gap, or over a 25-μm-deep trench, which is etched into the substrate as shown in Fig. 4. The MetalMUMPs process uses a six-mask process with eight thin-film layers.

Thermal isolation trenches are formed by opening windows in the silicon nitride layer, and potassium hydroxide (KOH) is used to etch 25 μm into the substrate. These trenches help improve thermal isolation to the substrate and improve dynamic performances due to enhanced convection.

The device prototypes have been made by using a minimum linewidth and space for the nickel structural layer equal to 8 μm. As one can see from the analytical model, device sensitivity is directly proportional to the length and inversely proportional to the beam's width and angle. The prototype has a beam length of 500 μm, a width of 10 μm, and beam angles equal to $\beta_1 = 14^\circ$ and $\beta_2 = 7^\circ$. These parameters were chosen based on optimization of the mathematical model.

The CoventorWare [19] software tool has been used in the device design phase to perform finite-element method (FEM) simulation, to simulate the etching results, and to design the mask layout. The simplified layout and a 3-D model of the cascaded bent-beam prototype are shown in Fig. 5. The interdigitated variable capacitor whose value depends on the environmental temperature is visible: The movable electrode is placed on the bent-beam apex, whereas the other electrode is fixed to the substrate.

A magnification of the circled areas in the device layout, at the left and right sides of the interdigitated apex, is reported in Fig. 6; it shows as the Vernier scales have been designed and realized to perform the temperature-to-apex-displacement characterization.

They have been placed on the opposite sides of the interdigitated capacitor with 5-μm shift so that, even if a maximum pitch of 10 μm can be designed with the proposed technology, a resolution of 5 μm can be obtained by looking at both sides.

Image processing has been used to allow measurements in displacement of fraction of micrometers under thermal excitation.

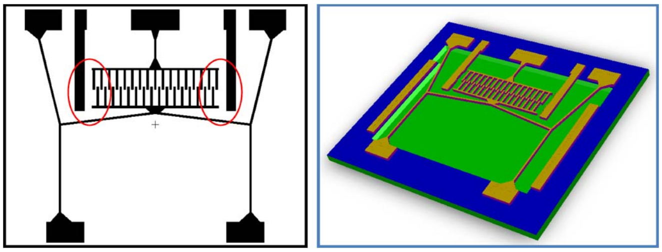

Fig. 5. (Left) Simplified layout showing only the metal mask used for defining the nickel areas. (Right) Three-dimensional view of the triple cascade bent-beam device prototype; both the variable capacitor and the Vernier scales are shown.

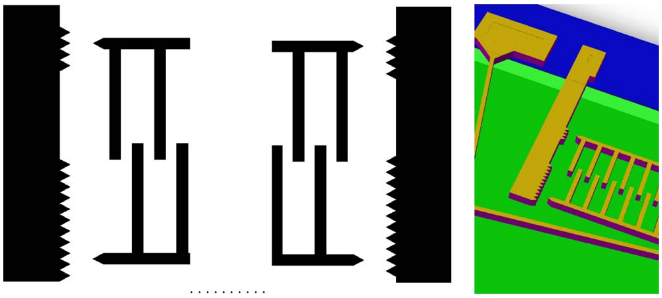

Fig. 6. Magnification of the structure in proximity of the Vernier scales. It has a pitch of 10 μm; however, the two sides have been shifted 5 μm to increase resolution.

The choice of the MetalMUMPs process has been dictated by mechanical requirements (for example, the achievable beam displacements) and the need to maximize the surface area of the interdigitated electrodes. MetalMUMPs allows a thick top nickel layer that other technologies, such as SOIMUMPs or PolyMUMPs [16], do not.

The nickel layer of the MetalMUMPs process exhibits also a high coefficient of thermal expansion, being approximately 13×10^{-6} K^{-1} [14]. Therefore, a very high sensitivity to temperature variation is obtained. On the other hand, the maximum operating temperature of nickel is about 623 K, and therefore, this value represents the upper boundary of the operating range of this device.

FEM simulations have been used to estimate both the displacement of the moving electrode in the interdigitated comb and the variation in capacitance through the Coventor "CoSolve" tool. In Fig. 7, the deformed shape of the triple bent beam is shown, and it is possible to observe that the

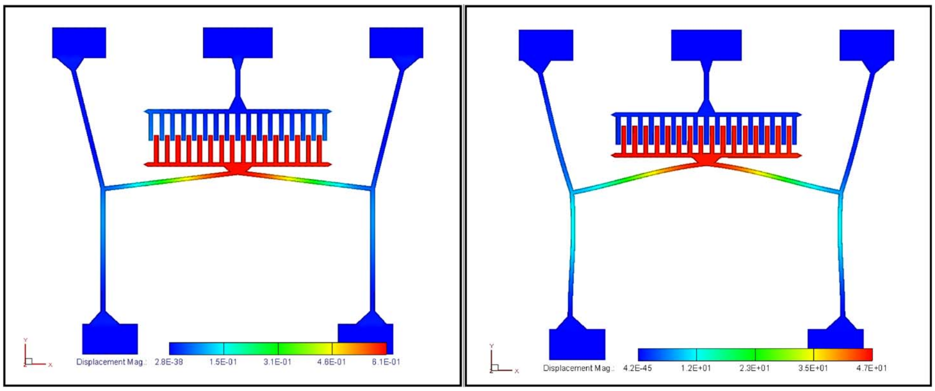

Fig. 7. Coventor simulation through CoSolve: Two results obtained (left) at 298 K and (right) at 500 K.

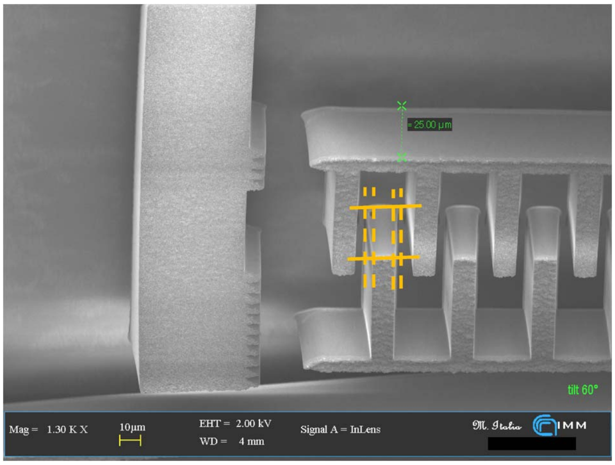

Fig. 8. SEM image of the interdigitated capacitor. From this picture, it is possible to evaluate the change in the finger thickness along their height (distance between the vertical dashed lines). This parameter is then taken into account in the analytical model.

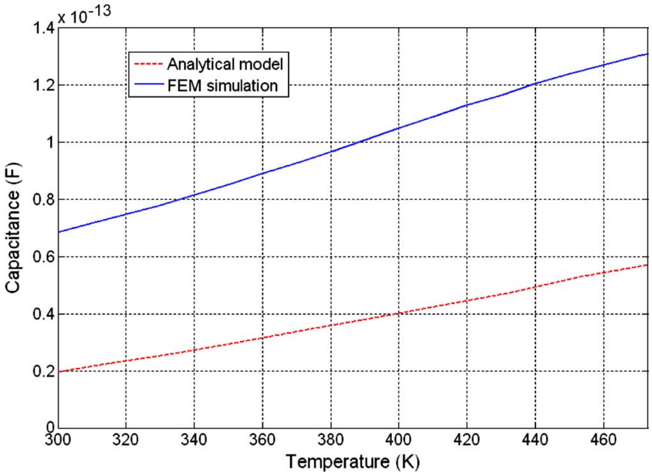

Fig. 9. Estimated capacitance variation obtained by finite-element analysis and analytical models.

overlap between interdigitated fingers changes significantly with temperature.

Comparisons of the results from FEM and analytical simulations are shown in Fig. 9 for the variation of capacitance with temperature.

In order to derive the analytical expression of the capacitance, we could consider the simple expression for a number of parallel conducting plates arranged into an interdigitated capacitor structure [20]; however, some considerations arise when considering experimental prototypes. In fact, if we consider Fig. 8, where a SEM image of the interdigitated capacitor fabricated is shown, it can be seen how, due to fabrication variation, the finger width changes with thickness. From Fig. 8, it is possible also to evaluate the width at the base of each finger and therefore also the air gap between fingers; in fact, this latter varies from 4 μm, at the bottom of the fingers, to the nominal 10 μm, on the top surface of the fingers.

The following equation has been therefore used to derive the analytical values of the interdigitated capacitance, considering that the etching process of the adopted technology does not lead to a rectangular profile but to a trapezoidal one, as shown in Fig. 8. Then, the temperature dependence of the capacitance can be expressed as

$$C(T) = 2N_{me}\varepsilon_0\varepsilon_r\left(y_0 + y(T)\right)\int_0^t \frac{dt_1}{x(t_1)} + (2N_{me}+1)\varepsilon_0\varepsilon_r\frac{(w_M + w_m)t}{2\left(g_{f0} - y(T)\right)} \quad (12)$$

where the variables are defined as follows.

- N_{me} is the number of fingers of the movable electrode (from the design, $N_{me} = 16$).
- y_0 is the initial overlap (engagement) between fingers at a temperature of 298 K (from the design, the theoretical value is $y_0 = 15\ \mu$m).
- y is the displacement of the movable electrode dependent on the temperature.
- t is the nickel layer thickness (from the technology parameters, $t = 20.5\ \mu$m).
- ε_0 is the dielectric constant of free space.
- ε_r is the relative dielectric constant.
- $x(t_1)$ is the lateral gap between fingers that is a function of the vertical dimension $\boldsymbol{t}$. It varies approximately linearly between 2 μm (at the bottom part of the fingers corresponding to a maximum beamwidth $w_M = 14\ \mu$m) and 10 μm (at the top part of the fingers corresponding to a minimum width $w_m = 10\ \mu$m): $x(t_1) = 4E - 6 + 2\,tg(\theta)\,t_1$ (for $0 < t_1 < t = 20.5\ \mu$m).

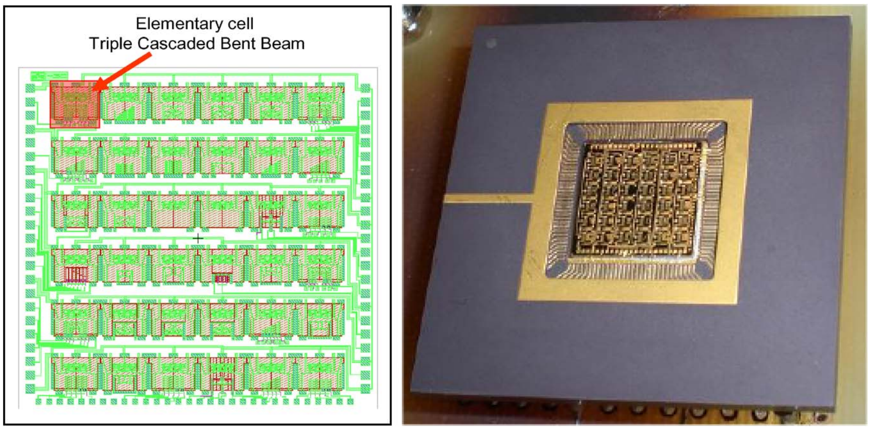

Fig. 10. (Left) Layout of a 10 mm × 10 mm MetalMUMPs die in which 36 identical elementary cells have been connected in parallel. (Right) Picture of the prototype in a standard 120-pin dual in-line ceramic package.

- The second term of (12) is for the capacitance to the frontal electrode; therefore, g_{f0} is the frontal gap at ambient temperature ($g_{f0} = 85\ \mu$m).
- The angle θ has been estimated from SEM images and suitable image processing procedures, leading to a value of about 8.7°.

The same trapezoidal profile has been also considered in FEM simulations. In Fig. 9, the capacitance values are reported as a function of temperature resulting from the FEM simulation and from the solution of (12). There, $y(T)$ is also obtained from numerical simulations.

From the previous numerical and analytical analysis, a sensitivity $S_{\mathrm{single}} = 0.35$ fF/K is obtained for the cascaded triple-bent-beam device shown in Fig. 7.

In order to enhance the device sensitivity to temperature changes, the basic capacitor cell can be replicated, and the outputs can be summed. In our case, we will proceed by designing and fabricating a 36-cell capacitor such that to have an estimated sensitivity equal to $S_{36} = 12.6$ fF/K.

IV. EXPERIMENTAL RESULTS

These devices have been fabricated by using the MetalMUMPs technology. In particular, 36 elementary cells as those described in Section III have been designed and connected in a parallel configuration in a 10 mm × 10 mm die, as shown in the left of Fig. 10. The right of Fig. 10 shows an image of the packaged microsystem.

A SEM picture of the fabricated device is shown in Fig. 11.

Measurements have been performed by applying a known temperature to the thermally controlled holder of an optical microscope, up to a maximum of 473 K (200 °C). Both the structure displacement and the capacitive variation have been characterized as a function of the temperature changes.

The fabricated Vernier scales have been taken as reference, and their relative positions are registered as shown in Fig. 12.

The experimental curve, represented in terms of the variation of the apex displacement as a function of the variation of temperature, has been derived, and it is shown in Fig. 13. In the same figure, the experimental results are compared with the expected behavior estimated through the analytical and the numerical FEM simulations.

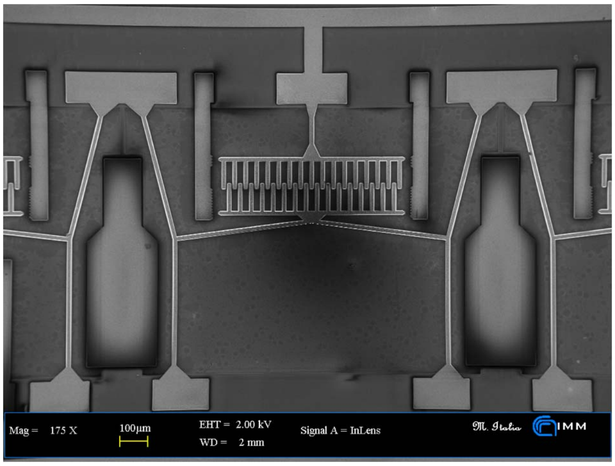

Fig. 11. SEM image of the fabricated cascade triple-bent-beam temperature transducer.

Fig. 13 shows the apex displacement as a function of the temperature considering small changes in angle β_2. A nonlinear response to the temperature change has been obtained with respect to the linear behavior shown in Fig. 3 assuming a constant value of β_2; in fact, as it is shown in Fig. 14, this angle changes significantly with the temperature and cannot be considered constant in the analytical model.

By taking into account this variation of the angle, a nonlinear output is obtained using the analytical model (this is also reported in [21] for a similar structure), and a very good agreement is obtained between the numerical simulation, the analytical calculations, and the experimental observations.

The second device characterization step has been focused on measuring the variation of the capacitance versus the variation of the temperature. A precision LCR meter (Agilent 4284A) has been used for the capacitive characterization. The minimum phase method has been adopted, whereas a working frequency of 1 kHz and a working amplitude of 10 mV have been set. The choice of these values comes from the considerations that the capacitive readout strategy has the inherent problem of interferences due to the electrostatic forces that arise between the two capacitive electrodes in response to the voltage applied to perform capacitance estimation. A quick evaluation of the forces in this system allows assessing that this voltage will

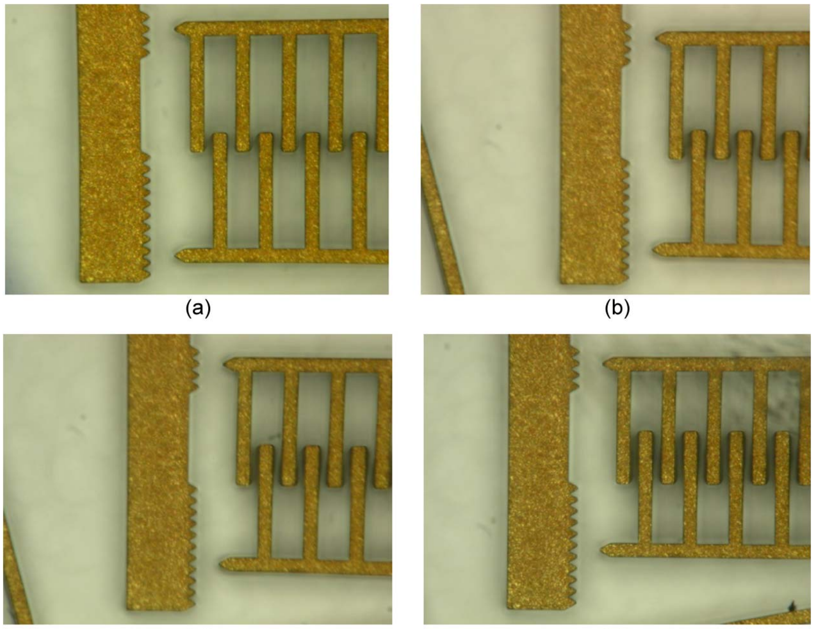
(a) (b)
(c) (d)

Fig. 12. Microscope pictures of the TCBB. (a) Vernier at 298 K. (b) Vernier at 353 K. (c) Vernier at 413 K. (d) Vernier at 473 K.

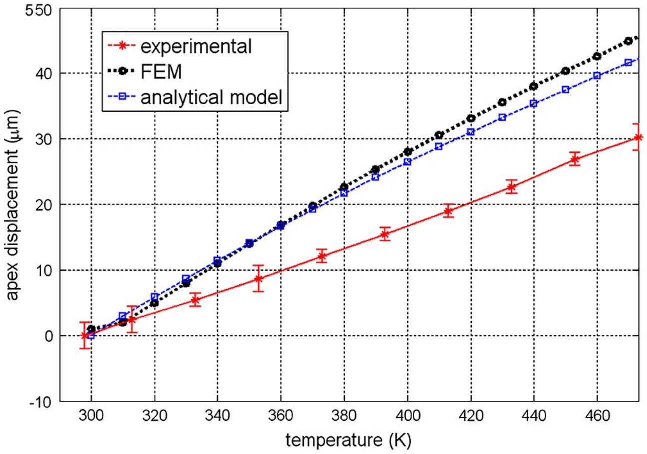

Fig. 13. Apex displacement as a function of temperature. The (bottom line) experimental results are reported together with the (center line) FEM and the (top line) analytical expectations.

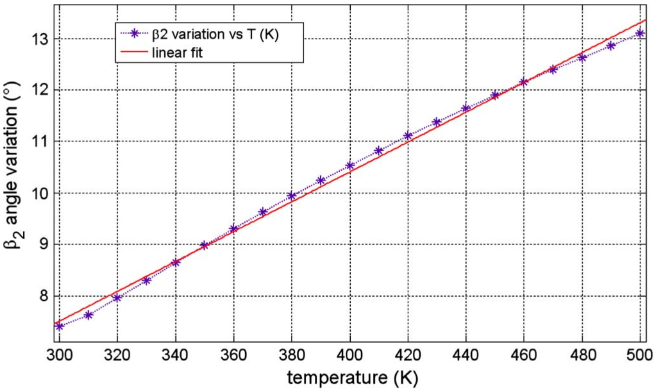

Fig. 14. Change of the angle in the triple-bent-beam structure with temperature.

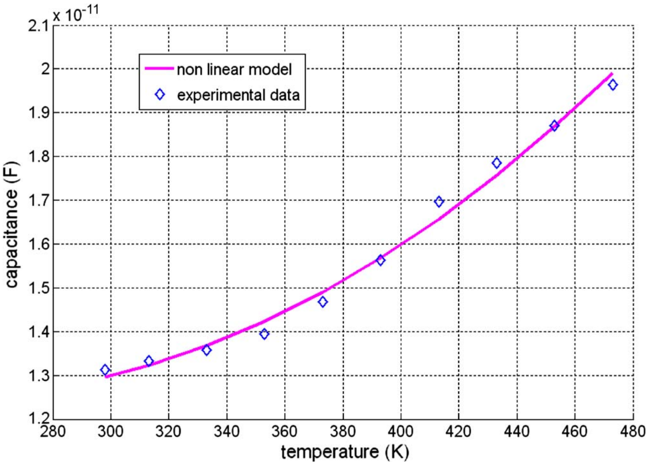

Fig. 15. Experimental measurement of the capacitance value against the temperature. In this figure, it is also shown the comparison of the experimental characteristic of the bent-beam (TCBB) temperature sensor and the capacitance $C^*(T)$ evaluated through (13) that takes into account the quadratic behavior.

induce electrostatic forces that are negligible with respect to those produced by thermal effects.

The capacitance variation has been obtained as a function of temperature variation, and it is shown in Fig. 15.

The experimental sensitivity in the first region of the response shown in Fig. 15 is $S_{36,\mathrm{sper}} \sim 12.66$ fF/K, in accordance with the theoretical result reported in Section III.

There are two main observations arising from the analysis of this figure: The capacitance value obtained is larger than what is expected from the model, and its response to the temperature is strongly nonlinear.

These behaviors may be explained in two ways. The capacitance nonlinearity is caused by the vertical misalignment of the fingers shown in Fig. 16(a), a consequent to the residual stress action, that produces a quadratic behavior; on the basis of these considerations, the analytical model reported in (13) has allowed the experimental data to be fitted using a quadratic

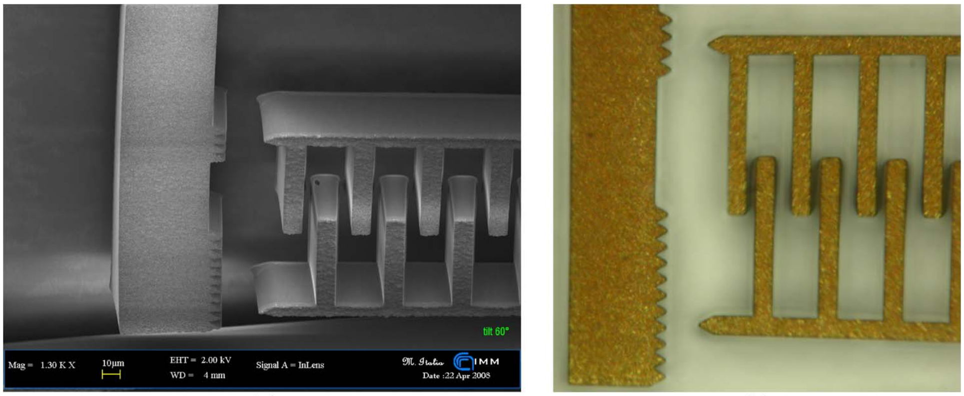

(a) (b)

Fig. 16. (a) SEM picture of the bent beam at room temperature. It is possible to see the finger vertical misalignment due to the structure residual stress. (b) Optical microscope image of the TCBB. Vernier at 393 K. Effect of the residual stress on the lateral misalignment observed in some cells.

function dictated by the contribution of the thermal expansion on both the width side and the thickness side

$$C^{*}(T)=2\cdot 36\cdot N_{me}\cdot\frac{s}{d}\cdot[y_0\cdot(1+\alpha_y T)]\cdot[t_0\cdot(1+\alpha_t T)]+c \tag{13}$$

where

N_{me}	number of fingers of the movable electrode ($N_{me}=16$);
y_0	initial experimental engagement between fingers at 298 K ($y_0=21.3$ μm);
t_0	initial experimental thickness whose value is known only at environmental temperature;
α_y, α_t	thermal expansion coefficients;
d	lateral gap (10 μm);
T	temperature variation (with respect to the environmental one);
c	constant value (to represent the offset experimentally observed deriving from the residual stress action).

A multidimensional unconstrained nonlinear minimization (Nelder–Mead) method [22] has been used to fit the experimental data with a quadratic function as that reported in (13). Coherently with the theoretical expectations, the following parameters have been estimated for this model: $\alpha_y = 2.47\times10^{-2}$ K^{-1}, $\alpha_t = 1.39\times10^{-2}$ K^{-1}, $t_0 = 18.4$ μm, and $c = 12.57$ pF. It can be seen that the two thermal expansion coefficients are of the same order of magnitude.

A lateral asymmetry observed for some cells of the device, as shown in Fig. 16(b), has the effect of enhancing both the capacitance value and its sensitivity to temperature changes, as reported also in [15], with respect to the theoretical and numerical analysis.

V. DESIGN OF THE INTEGRATED CONTACTLESS FRONT END

In order to address a contactless readout strategy, an electromagnetic energy transfer has been determined between the sensor capacitance, coupled to an inductor to comprise a resonant LC system, and a remote active transponder circuit. A layout draft of the whole passive LC integrated module is shown in Fig. 17. If, in these conditions, C_{sensor} is assumed to vary approximately in the range 13–19.6 pF, as it can be derived from Fig. 15, for T varying in the range 298 K–473 K, then a planar spiral (squared) inductor has been designed in the same MetalMUMPs technology.

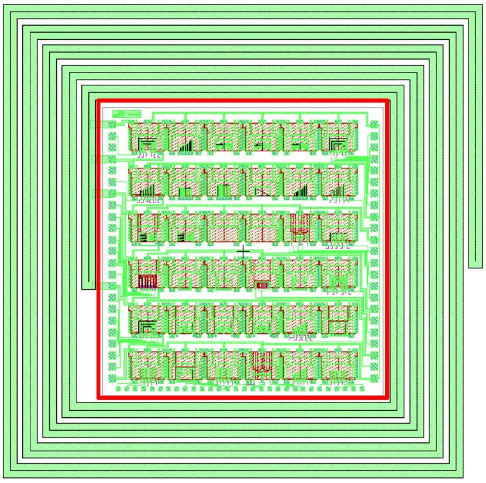

Fig. 17. Schematic setup of the integrated LC passive temperature sensor.

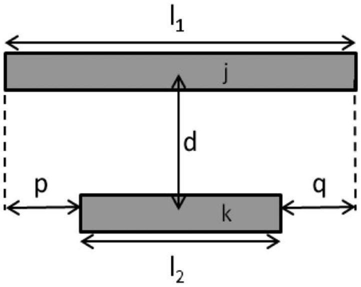

Fig. 18. Two conductor segments for mutual inductance calculations.

For modeling purposes, the inductance of a planar spiral structure is well calculated in [23] and [24]. Considering an inductor made of straight segments as shown in Fig. 18, the inductance is the sum of self-inductances and mutual inductances [24]

$$L_T = L_0 - M_{+} - M_{-} \tag{14}$$

where L_T is the total inductance, L_0 is the sum of self-inductances of all straight segments, M_{+} is the sum of positive mutual inductances, and M_{-} is the sum of negative mutual inductances.

The mutual inductance is the inductance resulting from the magnetic fields produced by adjacent conductors. It is positive when the directions of currents on conductors are in the same direction, and it is negative when the directions of currents are in opposite directions. The mutual inductance between two parallel conductors is a function of the length of the conductors and of the geometric mean distance between them. The mutual inductance of two conductors is calculated by

$$M = 2lF \text{ nH} \tag{15}$$

where l is the length of the conductor in centimeters and F is the mutual inductance parameter and is calculated as

$$F = \ln\left\{\left(\frac{l}{d}\right) + \left[1 + \left(\frac{l}{d}\right)^2\right]^{1/2}\right\} - \left[1 + \left(\frac{d}{l}\right)^2\right]^{1/2} + \left(\frac{d}{l}\right) \tag{16}$$

where d is the geometric mean distance between two conductors, which is approximately equal to the distance between the track centers of the conductors.

Then, in Fig. 18, j and k are the indices of the conductor, and p and q are the indices of the length for the difference in the lengths of the two conductors. Such a configuration (with partial segments) occurs many times along their perimeter for conductors in multiple-turn spiral inductors. The mutual inductance of conductors j and k in the aforementioned configuration is

$$\begin{aligned} M_{j,k} &= \frac{1}{2}\left\{(M_{k+p} + M_{k+q}) - (M_p + M_q)\right\} \\ &= \frac{1}{2}\left\{(M_j + M_k) - M_q\right\}, && \text{for } p = 0 \\ &= \frac{1}{2}\left\{(M_j + M_k) - M_p\right\}, && \text{for } q = 0 \\ &= M_{k+p} - M_p, && \text{for } p = q \\ &= M_k, && \text{for } p = q = 0. \end{aligned} \tag{17}$$

If the lengths of l_1 and l_2 are the same $(l_1 = l_2)$, then (17) is used. Each mutual inductance term in the aforementioned equation is calculated as follows by using (16) and (17):

$$M_{k+p} = 2l_{k+p}F_{k+p} \tag{18}$$

where

$$\begin{aligned} F_{k+p} = \ln&\left\{\left(\frac{l_{k+p}}{d_{j,k}}\right) + \left[1 + \left(\frac{l_{k+p}}{d_{j,k}}\right)^2\right]^{1/2}\right\} \\ &- \left[1 + \left(\frac{d_{j,k}}{l_{k+p}}\right)^2\right]^{1/2} + \left(\frac{d_{j,k}}{l_{k+p}}\right). \end{aligned} \tag{19}$$

The previous model has been implemented in a Matlab procedure. For the device considered in this work, a square planar spiral inductance has been designed. For a target resonance frequency of 10 MHz and $C = 13$ pF at ambient temperature, an inductance value of $L = 19.4$ μH is required.

The estimated parameters of such an inductor are as follows:

- number of turns $= 29$;
- metal width $= 100$ μm;
- metal spacing $= 20$ μm;
- inner diameter $= 10$ mm (equal to the 36-cell bent-beam capacitance area);
- outer diameter $= 16.9$ mm.

The layout of the whole device is shown in Fig. 16(b); there, the inductance diameter is to scale, whereas the inductance linewidth and spacing are not.

Then, if $L \sim 19.4$ μH is coupled to the variable capacitance, the resonance frequency of the LC circuit is varying approximately in the range $f_r \sim 10-8.15$ MHz. As a result, a variation of the resonance frequency $\Delta f_r \sim 1.85$ MHz is expected. This leads to a nominal sensitivity expressed as the variation of the resonance frequency as a function of the measurand (external temperature) of about

$$S_f \approx \frac{\Delta f_r}{\Delta T} \approx 10.6 \ \frac{\text{kHz}}{\text{K}}. \tag{20}$$

In conclusion, with a nominal resistivity of nickel equal to $8\ \mu\Omega \cdot \text{cm}$, a series resistance for the inductor must be taken into account. Its expected value is approximately equal to 61.2 Ω. Then, the quality factor Q of such an RLC circuit is approximately equal to 20.

VI. CONCLUSION

The development of a novel temperature sensor for contactless measurements has been described in this paper. Cascaded V-shaped bent-beam devices have been modeled, both analytically and numerically, and then designed and fabricated through the MetalMUMPs process.

The experimental characterization of the device behavior has been performed both in terms of displacement versus temperature change and in terms of capacitance variation versus temperature variation. The Vernier scales fabricated, together with the sensor, have been used for quantifying the device displacement by processing sequences of microscope images taken at different known temperatures; moreover, in order to avoid possible undesired effects of asymmetric motions on the results, a complete superposition and device shift procedure has been implemented from the sequence of microscope images.

In order to enhance the output signal, the single capacitive cell has been replicated into a 6 × 6 array.

The capacitance variation, as a function of the imposed temperature, has been separately characterized through different methods, including state-of-the-art LC meters or dedicated circuits.

Great efforts have been devoted here to gain a better understanding of the device behavior. In fact, even if the whole device is represented by a linear model and the displacement is linear with temperature, the measured output capacitance was nonlinear. This apparent contradiction was explored to gain complete knowledge of the system. The effects of process nonidealities on the capacitance response to temperature have been here discussed and modeled, closing the gap between the theoretical modeling and the experimental observations. Finally, referring to contactless readout, the design of an integrated inductor has been presented in order to realize an LC resonator that can be coupled with a remote readout circuit to sense the resonance frequency shift in response to temperature variation.

REFERENCES

[1] M. V. P. Kruger, M. H. Guddal, R. Belikov, A. Bhatnagar, O. Solgaard, C. Spanos, and K. Poolla, "Low power wireless readout of autonomous sensor wafer using MEMS grating light modulator," in *Proc. IEEE/LEOS Int. Conf. Opt. MEMS*, 2000, pp. 67–68.

[2] M. A. Fonseca, J. M. English, M. Von Arx, and M. G. Allen, "Wireless micromachined ceramic pressure sensor for high temperature applications," *J. Microelectromech. Syst.*, vol. 11, no. 4, pp. 337–343, Aug. 2002.

[3] M. A. Fonseca, M. G. Allen, J. Kroh, and J. White, "Flexible wireless passive pressure sensors for biomedical applications," in *Proc. Tech. Dig. Solid-State Sens., Actuators, Microsyst. Workshop*, Hilton Head Island, SC, Jun. 2006, pp. 37–42.

[4] E. Birdsell and M. G. Allen, "Wireless chemical sensors for high temperature environments," in *Proc. Tech. Dig. Solid-State Sens., Actuators, Microsyst. Workshop*, Hilton Head Island, SC, Jun. 2006, pp. 212–215.

[5] M. Suster, D. J. Young, and W. H. Ko, "Micro-power wireless transmitter for high-temperature MEMS sensing and communication applications," in *Proc. 15th IEEE Int. Conf. Micro Electro Mech. Syst.*, 2002, pp. 641–644.

[6] L.-H. Han and S. Chen, "Wireless bimorph micro-actuators by pulsed laser heating," *Sens. Actuators A, Phys.*, vol. 121, no. 1, pp. 35–43, May 2005.

[7] L. Que, J. S. Park, and Y. B. Gianchandani, "Bent-beam electro-thermal actuators for high force applications," in *Proc. 12th IEEE Int. Conf. MEMS*, Orlando, FL, Jan. 17–21, 1999, pp. 31–36.

[8] L. Que, J.-S. Park, and Y. B. Gianchandani, "Bent-beam electrothermal actuators—Part I: Single beam and cascaded devices," *J. Microelectromech. Syst.*, vol. 10, no. 2, pp. 247–254, Jun. 2001.

[9] J.-S. Park, L. L. Chu, A. D. Oliver, and Y. B. Gianchandani, "Bent-beam electrothermal actuators—Part II: Linear and rotary microengines," *J. Microelectromech. Syst.*, vol. 10, no. 2, pp. 255–262, Jun. 2001.

[10] Y. Shimamura, K. Udeshi, L. Que, J. Park, and Y. B. Gianchandani, "Impact behavior and energy transfer efficiency of pulse-driven bent beam electrothermal actuators," *J. Microelectromech. Syst.*, vol. 15, no. 1, pp. 101–110, Feb. 2006.

[11] Y. Zhang, Q.-A. Huang, R.-G. Li, and W. Li, "Macromodeling for polysilicon cascaded bent beam electrothermal microactuators," *Sens. Actuators A, Phys.*, vol. 128, no. 1, pp. 165–175, Mar. 2006.

[12] Y. B. Gianchandani and K. Najafi, "Bent-beam strain sensors," *J. Microelectromech. Syst.*, vol. 5, no. 1, pp. 52–58, Mar. 1996.

[13] L. L. Chu, L. Que, and Y. B. Gianchandani, "Measurements of material properties using differential capacitive strain sensors," *J. Microelectromech. Syst.*, vol. 11, no. 5, pp. 489–498, Oct. 2002.

[14] B. Andò, S. Baglio, N. Pitrone, N. Savalli, and C. Trigona, "Bent beam MEMS temperature sensors for contactless measurements in harsh environments," in *Proc. IEEE I ^{2}MTC*, Victoria, BC, Canada, May 12–15, 2008, pp. 1930–1934.

[15] M. Serpelloni, D. Marioli, E. Sardini, B. Andò, S. Baglio, N. Savalli, and C. Trigona, "An hybrid telemetric MEMS for high temperature measurement into harsh industrial environment," in *Proc. IEEE I ^{2}MTC*, Singapore, May 5–7, 2009, pp. 1423–1428.

[16] B. Hardy, Introduction to MEMSCAP and MUMPs. [Online]. Available: http://www.stimesi.org/

[17] S. P. Timoshenko and J. M. Gere, *Mechanics of Materials*, 3rd ed. Boston, MA: PWS, 1990, pp. 632–647.

[18] N. Lobontiu and E. Garcia, *Mechanics of Microelectromechanical Systems*. Boston, MA: Kluwer, 2004, pp. 368–379.

[19] Success in MEMS Manufacturing. [Online]. Available: http://www.coventor.com/pdfs/Success_in_MEMS_Manufacturing.pdf

[20] R. Pallás-Areny and J. G. Webster, *Sensors and Signal Conditioning*, 2nd ed. New York: Wiley-Interscience, 2001, ch. 4.

[21] Y. Zhang, Q.-A. Huang, R. G. Li, and W. Li, "Macro-modeling for polysilicon cascaded bent beam electrothermal microactuators," *Sens. Actuators A, Phys.*, vol. 128, no. 1, pp. 165–175, Mar. 2006.

[22] J. A. Nelder and R. Mead, "A simplex method for function minimization," *Comput. J.*, vol. 7, no. 4, pp. 308–313, Jan. 1965.

[23] V. G. Welsby, *The Theory and Design of Inductance Coils*. New York: Wiley, 1960.

[24] H. M. Greenhouse, "Design of planar rectangular microelectronic inductors," *IEEE Trans. Parts, Hybrids, Packag.*, vol. PHP-10, no. 2, pp. 101–109, Jun. 1974.

Bruno Andò received the M.S. degree in electronic engineering and the Ph.D. degree in electrical engineering from the University of Catania, Catania, Italy, in 1994 and 1999, respectively.

From 1999 to 2001, he was a Researcher with the Electrical and Electronic Measurement Group, Dipartimento di Ingegneria Elettrica Elettronica e dei Sistemi, University of Catania, where he has been an Assistant Professor since 2002. During his activity, he has coauthored several scientific papers, presented in international conferences and published in international journals and books. His main research interests are sensor design and optimization, advanced multisensor architecture for ambient assisted living, sensor networks, characterization of new materials for sensors, nonlinear techniques for signal processing with particular interest in stochastic resonance and dithering applications, and distributed measurement systems.

Salvatore Baglio (S'93–M'95–SM'03) received the Laurea and Ph.D. degrees from the University of Catania, Catania, Italy, in 1990 and 1994, respectively.

Since 1996, he has been with the Dipartimento di Ingegneria Elettrica Elettronica e dei Sistemi, University of Catania, where he is currently an Associate Professor. He teaches courses in "measurement theory," "electronic instrumentations," and "integrated microsensors." He is a coauthor of more than 250 scientific publications, including books, chapters in books, papers in international journals, and proceedings of international conferences. He is also the holder of several U.S. and European patents. His research interests are mainly focused on micro- and nanotechnologies, micro- and nanosensors, hysteretic materials for sensors, and nonlinear dynamics for transducers.

Prof. Baglio has served as Associate Editor for the IEEE TRANSACTIONS ON CIRCUITS AND SYSTEMS and as Distinguished Lecturer for the IEEE Circuits and Systems Society. He is currently an Associate Editor of the IEEE TRANSACTIONS ON INSTRUMENTATION AND MEASUREMENT and the Chair of the IEEE Instrumentation and Measurement Society Italy Chapter.

Nicolò Savalli received the M.S. and Ph.D. degrees from the University of Catania, Catania, Italy, in 1999 and 2003, respectively.

Since 2003, he has been a Lecturer of applied electronic measurements and electrical measurements with the Dipartimento di Ingegneria Elettrica Elettronica e dei Sistemi, University of Catania, where he is currently a Research Associate. He is a coauthor of more than 100 scientific publications, including international journals, international conferences, and national conferences. His main research interests include instrumentation and measuring systems, smart sensors, material characterization, microsensors and microsystems in standard and dedicated technologies, photonic band-gap materials, and optical filters.

Carlo Trigona was born in Siracusa, Italy, on December 18, 1981. He received the M.S. degree in automation engineering and control of complex system and the Ph.D. degree in electronic, automation and control of complex system from the University of Catania, Catania, Italy, in 2006 and 2009, respectively.

He is currently with the Dipartimento di Ingegneria Elettrica Elettronica e dei Sistemi, University of Catania. He is the author of several scientific papers. His research interests include microsystems and microsensors, fluxgate magnetometers, and analog and digital electronic circuit design.